

A compression scheme for radio data in high performance computing

Kiyoshi Masui^{a,b,*}, Mandana Amiri^a, Liam Connor^{c,d,e}, Meiling Deng^a, Mateus Fandino^a, Carolin Höfer^a, Mark Halpern^a, David Hanna^f, Adam D. Hincks^a, Gary Hinshaw^a, Juan Mena Parra^f, Laura B. Newburgh^d, J. Richard Shaw^{a,c}, Keith Vanderlinde^{e,d}

^aDepartment of Physics and Astronomy, University of British Columbia, 6224 Agricultural Rd. Vancouver, V6T 1Z1, Canada

^bCanadian Institute for Advanced Research, CIFAR Program in Cosmology and Gravity, Toronto, ON, M5G 1Z8

^cCanadian Institute for Theoretical Astrophysics, 60 St George St, Toronto, ON, M5S 3H8, Canada

^dDunlap Institute for Astronomy & Astrophysics, University of Toronto, 50 St George St, Toronto, ON, M5S 3H4, Canada

^eDepartment of Astronomy & Astrophysics, University of Toronto, 50 St George St, Toronto, ON, M5S 3H4, Canada

^fDepartment of Physics, McGill University, 3600 University St, Montreal, Canada

Abstract

We present a procedure for efficiently compressing astronomical radio data for high performance applications. Integrated, post-correlation data are first passed through a nearly lossless rounding step which compares the precision of the data to a generalized and calibration-independent form of the radiometer equation. This allows the precision of the data to be reduced in a way that has an insignificant impact on the data. The newly developed **Bitshuffle** lossless compression algorithm is subsequently applied. When the algorithm is used in conjunction with the HDF5 library and data format, data produced by the CHIME Pathfinder telescope is compressed to 28% of its original size and decompression throughputs in excess of 1 GB/s are obtained on a single core.

Keywords:

radio astronomy, data compression, HDF5, high performance computing

1. Introduction

The simultaneous drives to wider fields and higher sensitivity have led radio astronomy to the cusp of a big-data revolution. There is a multitude of instruments, including 21 cm cosmology experiments [1–9], Square Kilometer Array Precursors [10–12], and ultimately the Square Kilometer Array [13], whose rate of data production will be orders of magnitude higher than any existing radio telescope. An early example is the CHIME Pathfinder [14, 15] which will soon be producing data at a steady rate of over 4 TB per day. The cost associated with storing and handling these data can be considerable and therefore it is desirable to reduce the size of the data as much as possible using compression. At the same time, these data volumes produce a significant data processing challenge. Any data compression/decompression scheme must be fast enough as to not hinder data processing, and would ideally lead to a net increase in performance due to the reduced time required to read the data from disk.

Here, after discussing some general considerations for designing data storage formats in Section 2, we present a scheme for compressing astronomical radio data. Our procedure has two steps: a controlled (relative to thermal noise) reduction of the precision of the data which reduces

its information entropy (Section 3), and a lossless compression algorithm—**Bitshuffle**¹—which exploits this reduction in entropy to achieve a very high compression ratio (Section 4). These two steps are independent in that, while they work very well together, either of them can be used without the other. When we evaluate our method in Section 5 we show that the precision reduction improves compression ratios for most lossless compressors. Likewise, **Bitshuffle** outperforms most other lossless compressors even in the absence of precision reduction.

2. Considerations for designing data storage formats

2.1. Characteristics of radio-astronomy data and usage patterns

Integrated, post-correlation radio-astronomy data are typically at least three dimensional, containing axes representing spectral frequency, correlation product, and time². The *correlation product* refers to the correlation of all antenna input pairs, including auto-correlations and cross-correlations between different polarisations from the same

¹<https://github.com/kiyo-masui/bitshuffle>

²A fourth axis is often introduced when data are ‘folded’ or ‘gated’—i.e., if data from the on- and off-periods of a switched, calibration noise source are accumulated separately, or pulsar data is folded on the pulsar’s period which is divided into many gates.

*Corresponding author, kiyo@physics.ubc.ca

antenna. In a single dish these form the polarization channels for each beam and in an interferometer these are the visibilities. This also applies to beam forming interferometers, where linear combinations of antenna inputs are formed (either in analog or digitally) before correlation.

The CHIME collaboration determined that its data are most commonly accessed along the time axis. That is, it is generally most efficient for the axis representing time to be the fastest varying once loaded into memory. This is the case for noise characterisation, radio-frequency interference (RFI) flagging and system-health monitoring, to name a few. Most importantly, the map-making pipeline typically produces maps on a per-frequency basis and is most efficient at processing time-contiguous data. Though it is sometimes necessary to work with spectra (slices along the frequency axis) or ‘correlation triangles’ (slices along the correlation product axis), we find that these use cases normally only involve a few slices and large I/O operations in these spaces are rare.

Of course, the CHIME collaboration’s preference for the time axis to be the fastest varying will not apply to all consumers of radio data. One expects that access patterns might vary considerably for the diverse applications of radio data, including spectroscopy, synthesis imaging, and pulsar timing. But as discussed below, arranging data with time as the fastest varying index is beneficial for data compression.

2.2. Compression: benefits and requirements

Compression can greatly ease the burden of storing and handling large data sets, but there are also performance benefits. Compression algorithms exist whose decompression cost is negligible compared to the cost of reading from disk. As we will show, data may be compressed by up to a factor of four in some cases. As such, the time required to load a dataset from disk into memory may be reduced by a factor of four using compression.

We previously stated that ordering data with the axis representing time as the fastest varying is most efficient for the majority of I/O operations. This ordering is also beneficial for compression, since adjacent data points are likely to be highly correlated, presuming that the cadence is such that the spatially-smoothly varying sky is Nyquist sampled. On the other hand, it is most natural to record data with time as the *slowest* varying index since that is the order in which they are generated by the instrument. To have time as the fastest varying index, the data must either be buffered in memory (which is impractical), written with strided writes (which is inefficient) or reordered after acquisition. Since the data are acquired and written only once but read many times, it is logical to prioritise read-performance over write-performance. Thus, the CHIME collaboration deemed a post-acquisition reordering step to be worthwhile.

The same argument can be used to prioritise data decompression speed over compression speed. Compression is sufficiently cheap computationally that even a modest

number of processors should be able to keep up with the acquisition rate of CHIME Pathfinder data (which will be ~ 50 MiB/s depending on runtime parameters) for almost any compression algorithm. Even if this were not the case, data could be compressed in parallel post acquisition. On the other hand, one might wish to load several days of acquired data at once for analysis, and ideally, this would be bound only by disk read times, not decompression speed.

The decompression cost may not be negligible compared to read times for files that are cached in memory or stored on high-performance parallel file systems. This makes it desirable to have as fast a decompression scheme as possible as the benefits of speed are not always limited by hard drive access. A multi-threaded implementation of the decompression algorithm can thereby result in a significant speed up on multi-core systems.

To summarise all of the foregoing, the following requirements for a compression scheme emerge:

Unbiased Any lossy compression must not bias the data in any way.

Nearly lossless Any lossy compression employed must be controlled in a manner that is *guaranteed* not to significantly decrease the sensitivity of the data.

Time minor In the multi-dimensional dataset, the axis representing time should be the fastest varying. This allows for the efficient reading of small subsets of spectral frequencies and correlation products but for large periods of time.

Fast decompression To realize the performance gains associated with compressing the data, we require the time to decompress the data to be small compared to the time required to read the data from disk. At the time of writing, a single hard drive can typically be read at a rate of ~ 100 MiB/s. As such, a compression algorithm with throughput of ~ 1 GiB/s on a single processor is desirable.

Threaded When using a parallel file system, or when the file is cached in system memory, reading throughputs can be much higher compared to when using a single hard disk. For decompression to not degrade performance in these cases, the compression library should be threaded.

Thread-safe While the HDF5 library (see Section 2.3, below) is not internally threaded, it may become so in the future. In addition, programs may attempt to hide the cost of IO operations by putting them in a separate thread. The compression library must therefore be thread-safe.

2.3. HDF5 and chunked storage

The Hierarchical Data Format 5 (HDF5) [16] is a widely used data format in astronomy, capable of storing and organizing large amounts of numerical data. In the context

of this paper, it also has the benefit of allowing for ‘chunked storage’. That is, an HDF5 ‘dataset’—a multidimensional array of homogeneous type—can be broken up into subsets of fixed size, called chunks, which are stored in any order on disk, with locations recorded in a look-up table. This is in contrast to contiguous storage, in which random access is obviously trivial. The advantage of chunked storage for our purposes is that though the number of elements in a chunk is fixed, its size is not, and as such it may readily be compressed.

The primary drawback of chunked storage is that full chunks must be read from disk at a time. As such, to read a single array element, the full chunk containing thousands of elements must be read. In practice, this is mitigated by the fact that hard disk latencies are very long compared to the time required to read data from disk. Typically a chunk of several hundred KiB can be read from disk in only twice the time required to read a single element of a contiguous dataset, and thus the cost of chunked storage for random access is at most a factor of two, as long as chunk sizes are chosen appropriately. In addition, requiring a large number of random accesses to a dataset is a rare usage case for radio data, and therefore random access performance should rarely be a driving factor when designing a data format.

HDF5 implements compression of chunked datasets via a ‘filter pipeline’. Any number of filters can be specified when the dataset is created. When a data chunk is to be stored, the buffer is sequentially passed through filter functions before being written to disk. When the chunk is to be read from disk, it is passed through the inverse filter functions in reverse order before being presented to the user. Many HDF5 filters are available whose functions include lossless and lossy compression, preconditioning filters aimed at improving compression ratios, and other utilities such as data check-sums. The filter-pipeline is also extensible, and writing a new filter, such as the one presented in this paper, is a relatively straightforward task.

3. Lossy entropy reduction: reduction of precision

All experiments must perform some amount of lossy compression simply by virtue of having to choose a finite width data type which reduces precision by truncation. Here, we focus on performing a reduction of precision in a manner that is both controlled, in that it has a well-understood effect on the data; and efficient, in that only the required precision is kept allowing for better compression.

Reducing the precision of the data involves discarding some number of the least significant bits of each data element whose significance is small compared to the noise. For integers, this is accomplished by rounding values to a multiple of a power of two. For floating point numbers the equivalent operation is performed on the significand part of the value, however in this work we focus on integer data. In some cases this may allow for data to fit

into a smaller data type, for example single-precision (32-bit) as opposed to double-precision (64-bit) floating point numbers. However, even if this is not the case it is still beneficial to identify bits that are well within the noise margin and replace them with zeros. Bits that are dominated by noise are essentially random and are thus very high entropy. Any subsequent lossless compression has no hope of compressing them despite their insignificance.

Of course for this to be useful, it is necessary for the lossless compression step to be able to exploit the reduced entropy associated with zeroing the noisy bits. This will be discussed in Section 4.

In this section, we begin with a discussion of noise for a general radio dataset. We derive an expression for the thermal noise, including possible correlated components from the sky (so-called self-noise), that is independent of calibration. We then use this estimate to derive an acceptable level of rounding, specified by the rounding granularity, such that the induced error and thus rounding noise is negligible compared to thermal. The final result is a procedure for rounding the data elements that maximizes the reduction of entropy of the data while constrained to fixed loss of sensitivity.

3.1. Noise and the radiometer equation

Any discussion of reducing numerical precision must necessarily include a discussion of noise, the intrinsic scatter in the data independent of any discretization effects. If the error induced by reducing the precision of the data is small compared to the scatter from the noise, then the reduction will have a negligible effect on the data, assuming the error is unbiased. Here, we will focus on thermal noise which is present for all sources of incoherent radiation and is thus a lower limit on the noise present in the data. Thermal noise causes uncertainty in the measurement of radiation power that is proportional to that power. It is due to the stochastic nature of incoherent radiation. Coherent sources of radiation can increase the measured power without increasing scatter, however such sources are rare in astronomy. Radio-frequency interference, however, may be coherent.

Fortunately the thermal noise can be estimated from the data on a sample-by-sample basis, and independently of any calibration factors, using the radiometer equation. Usually it is assumed that the thermal noise is uncorrelated between correlation products, but we will show that the noise is in general correlated and will compute the associated covariance matrix. We will argue that in some observational regimes it may be necessary to take these correlations into account when reducing the numerical precision of the data relative to the noise.

We denote the correlation products in a single spectral bin and in a single time integration as $V_{ij} \equiv \langle a_i a_j^* \rangle$, where a_i is the digitized and Fourier-transformed signal from antenna channel i , and the angular brackets are an ensemble average which is approximated using a time average within the integration time. The noise is charac-

terized by the covariance matrix of the full set of correlation products, $C_{\alpha ij, \beta gh}$. Here, the indices i, j, g , and h run over the antenna number and α and β run over the real and imaginary parts. For example $C_{\text{Re } ij, \text{Im } gh} \equiv \langle \text{Re } V_{ij} \text{Im } V_{gh} \rangle - \langle \text{Re } V_{ij} \rangle \langle \text{Im } V_{gh} \rangle$.

It is typically assumed that the cross-correlations between channels are much smaller than the auto-correlations, i.e. $V_{ij}V_{ij}^* \ll V_{ii}V_{jj}$ for $i \neq j$. This is because it is assumed that the total measured power is dominated by noise from the amplifiers in the signal chain prior to digitization. In this limit, all correlation products are uncorrelated and the well known radiometer equations are [17, chap. 6.2]

$$\sigma_{\text{Re } ii}^2 = \frac{V_{ii}^2}{N}, \quad (1)$$

$$\sigma_{\text{Im } ii}^2 = 0, \quad (2)$$

$$\sigma_{\alpha ij}^2 = \frac{V_{ii}V_{jj}}{2N} \quad (i \neq j). \quad (3)$$

Here $N = \Delta_\nu \Delta_t$ is the number of samples entering the integration, and one notes that the auto-correlations, V_{ii} , are purely real. These can be aggregated into a diagonal covariance matrix:

$$C_{\alpha ij, \beta gh} = \delta_{\alpha\beta}(\delta_{ig}\delta_{jh} + \delta_{ih}\delta_{jg})(1 - \delta_{ij}\delta_{\alpha\text{Im}})\frac{V_{ii}V_{jj}}{2N}, \quad (4)$$

where δ_{ij} is the Kronecker delta which is unity for $i = j$ and zero otherwise. The first factor in parentheses just cancels the factor of two for auto-correlations and accounts for the fact that $V_{ij} = V_{ji}^*$. The second factor in parentheses sets the whole expression to zero for the imaginary part of the auto-correlations.

Equation 4 is appropriate in many observational regimes and is the equation we use for CHIME data. However, there are cases when the correlation products can be highly correlated. With the recent increased emphasis on low spectral frequencies (where sky brightness typically dominates over amplifier noise) and on close packed arrays (where amplifier noise may become coupled between channels) the approximation that the cross-correlations are small may not hold. A more general set of equations describing the noise is [18]:

$$C_{\text{Re } ij, \text{Re } gh} = \frac{1}{2N} \text{Re} [V_{ig}V_{jh}^* + V_{ih}V_{jg}^*], \quad (5)$$

$$C_{\text{Im } ij, \text{Im } gh} = \frac{1}{2N} \text{Re} [V_{ig}V_{jh}^* - V_{ih}V_{jg}^*], \quad (6)$$

$$C_{\text{Re } ij, \text{Im } gh} = \frac{1}{2N} \text{Im} [-V_{ig}V_{jh}^* + V_{ih}V_{jg}^*]. \quad (7)$$

These may be derived from first principles by Wick expanding the four-point correlations of a_i in terms of the correlation products V_{ij} .

Below we show some special cases of the above equa-

tions to illustrate how they differ from Equation 4.

$$C_{\text{Re } ii, \text{Re } ii} = \frac{1}{N} V_{ii}^2 \quad (8)$$

$$C_{\text{Im } ii, \text{Im } ii} = 0 \quad (9)$$

$$C_{\text{Re } ii, \text{Re } ij} = \frac{1}{N} V_{ii} \text{Re}(V_{ij}) \quad (10)$$

$$C_{\text{Re } ij, \text{Re } ij} = \frac{1}{2N} [V_{ii}V_{jj} + \text{Re}(V_{ij})^2 - \text{Im}(V_{ij})^2] \quad (11)$$

$$C_{\text{Im } ij, \text{Im } ij} = \frac{1}{2N} [V_{ii}V_{jj} - \text{Re}(V_{ij})^2 + \text{Im}(V_{ij})^2] \quad (12)$$

$$C_{\text{Re } ij, \text{Im } ij} = \frac{1}{N} [\text{Re } V_{ij} \text{Im } V_{ij}] \quad (13)$$

One would expect that it is the diagonal of this covariance matrix, $C_{\alpha ij, \alpha ij}$, to which the error associated with precision reduction should be compared. These diagonal elements give the variance of a data element marginalized over all other elements. It is actually more appropriate to compare the error to the unmarginalized variance, that is $1/(C^{-1})_{\alpha ij, \alpha ij}$. If the truncation error is small compared to the marginalized variance then the ability to measure an individual visibility will be unaffected, while if the error is small compared to the unmarginalized variance, then the ability to measure any linear combination of correlation products will be unaffected. The two expressions are equivalent if using Equation 4 for the covariance but may differ significantly when the data are dominated by the sky instead of receiver-noise.

As an illustrative example of how the noise can be highly correlated between correlation products, consider the case of an interferometer where the visibilities are dominated by a single unresolved point source. For simplicity, we assume the source is at zenith and that the gains and phases of all inputs are calibrated, although our argument does not depend on this. For these conditions, the real parts of all visibilities are equal and proportional to the source flux, while the imaginary parts are zero. As shown in Kulkarni [18], the noise is dominated by the so-called self-noise. All the elements of the (Re Re) block of the covariance matrix are also equal, indicating that the visibilities are perfectly correlated and that there is only one effective measurement of the source. However, the variance of the difference between any two visibilities is zero. The difference of the two visibilities is essentially a new correlation product whose effective beam has a null at the zenith. So while the auto-correlations and thus the variance of the visibilities are dominated by the source, any linear combination of visibilities whose effective beam does not include the source will have much lower noise.

When defining the matrix \mathbf{C} , it is necessary to note that there are several redundant combinations of indices for the correlation products. The (Re ij) index is equivalent to the (Re ji) element, and the (Im ij) and (Im ji) correlation products are related by a negative sign. In addition the (Im ii) correlation products are identically zero, carry no information, and have no noise. The rows and

columns of \mathbf{C} associated with these correlation products should be discarded. However, after removing this redundancy, \mathbf{C} is guaranteed to be at least positive semi-definite and, as long as the system temperature is finite, positive definite and thus invertible. Only non-linearity in the *correlator* (not the analog systems or ADCs) can render it non-invertible.

Unfortunately, for interferometers with more than a few dozen elements, it is not feasible to invert the covariance matrix for every spectral bin and every temporal integration in real time. As such, for large interferometers, we must fall back to using Equation 4 over Equations 5–7. While not strictly accurate, Equation 4 remains an excellent approximation for most observational regimes. For CHIME, no source on the sky other than the sun increases the total power by more than roughly 40% at any spectral frequency. Since the errors from precision reduction will be sub-dominant to the noise by several orders of magnitude, even order unity mis-estimations of the noise should have negligible impact on the final data. Nonetheless, one may want to compensate for this error by being extra conservative when specifying the degree of precision reduction as will be discussed in the next section.

For the remainder of this paper we will define the RMS noise used to calculate truncation precision as

$$s_{\alpha ij} \equiv \sqrt{1/(C^{-1})_{\alpha ij, \alpha ij}}, \quad (14)$$

with \mathbf{C} defined in either Equation 4 or Equations 5–7 depending on interferometer size.

3.2. Rounding the data relative to the noise

With an expression in hand for $s_{\alpha ij}$, which is our basis for comparison when adding numerical noise, we can proceed to derive a procedure for rounding the data values. In this section we will drop the indices on s with the procedure being understood to apply on a correlation product by correlation product basis.

We will be relating s to the rounding granularity g , which is the power of two to a multiple of which we will be rounding each data element. Note that by rounding instead of simply truncating, one extra bit can be discarded for essentially no cost since the induced error associated with zeroing a given number of bits is half as large. Rounding also has the very desirable property of being unbiased³, provided the data values are randomly distributed within the granularity (which is an excellent approximation since the granularity will be much smaller than the Gaussian thermal noise). This is not true of truncation, where the bias is half the granularity.

We define σ_r^2 as the added noise variance associated with reducing the precision of a data element. We will require that $\sigma_r^2 < fs^2$, where f is the maximum fractional increase in noise from precision reduction. It can

be thought of as the effective fractional loss of integration time caused by reducing the precision.

When using the approximate Equation 4 in the definition of s , the approximation can be compensated for by reducing f by a factor of the minimum portion of total power originating from receiver-noise squared. To be more precise, multiplying f by the minimum of $1 - V_{ij}V_{ij}^*/(V_{ii}V_{jj})$ (for $i \neq j$), roughly compensates for the approximation. This will be especially relevant to low-frequency compact arrays with many elements, for reasons mentioned above. This could in principle be performed dynamically as a function of time or spectral frequency, although no attempt is made to implement this.

For randomly distributed rounding errors (which is an excellent approximation since the rounding will occur in noise-dominated bits), the rounding noise is related to the granularity by [20]:

$$\sigma_r^2 = g^2/12. \quad (15)$$

Thus the *maximum rounding granularity* is:

$$g < \sqrt{12fs^2}, \quad (16)$$

Our precision-reduction scheme is to round each data element to a multiple of the largest possible power of two, g , subject to the constraint given in Equation 16. We note that this equation gives an upper limit, and that on average the granularity and added noise will be below this limit.

For maximum generality, the set of $s_{\alpha ij}$ should be recalculated for each spectral frequency and each temporal integration, allowing the precision reduction to adapt to sky and bandpass spectral structure, temporal changes in the sky, and time and frequency dependant RFI.

When using Equation 4 for the noise, the calculation of $s_{\alpha ij}$ requires only a handful of floating point operations per data-element and thus has negligible cost compared to the initial correlation. Finding the largest integer power-of-two granularity that satisfies Equation 16 and then rounding to that granularity can be performed in tens of instructions with no branching. An example implementation in the Cython programming language is available online⁴.

As discussed above, performance is a greater concern for decompression than compression. The precision reduction requires no decoding, and as such its throughput is of secondary concern. The example implementation is only lightly optimized and achieves ~ 300 MiB/s throughput on a single core of a modern processor. This was deemed sufficient for CHIME’s data acquisition, although we hypothesize that a factor of four speed-up may be possible by employing the vectorized SSE instruction sets.

The precision reduction applied to the data shown in Figure 1 is illustrated in the first two panels of Figure 2.

³We choose the ‘round ties to even’ tie breaking scheme [19], which is unbiased.

⁴<https://gist.github.com/kiyo-masui/b61c7fa4f11fca453bdd>

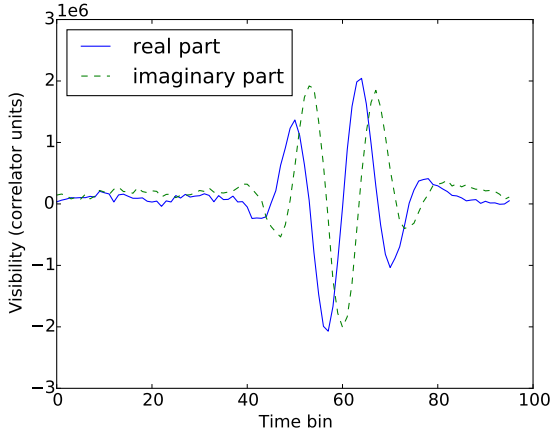


Figure 1: Example visibility data for an inter-cylinder baseline of the CHIME Pathfinder: 96 10 s-integrations of a 0.39 MHz wide spectral bin at 644 MHz.

4. Lossless compression: Bitshuffle

Here we discuss lossless data compressors in the context of radio astronomical data. We seek a compressor that is fast enough for high performance applications but also obtains high compression ratios, especially in the context of the precision reduction discussed in the previous section. Satisfying both criteria is difficult and existing compressors are found to be inadequate. Therefore, a custom compression algorithm, **Bitshuffle**, was developed; it is both fast and obtains high compression ratios, at the expense of being slightly less general.

In this section we begin by reviewing popular algorithms, some understanding of which is necessary to motivate the design of **Bitshuffle**. We then describe the **Bitshuffle** algorithm, its interaction with the precision reduction step, and its implementation.

4.1. Brief description of popular lossless compression algorithms

By far, the most common class of compression algorithms is the LZ77 class of encoders [21, 22]. These include LZ77, LZF⁵, LZ0⁶, Google’s Snappy⁷, LZ4⁸ and others. The LZ77 encoders compress data by searching for repeated sequences of bytes in the uncompressed data stream. When a sequence that occurred earlier in the stream is found it is replaced by a reference to the earlier occurrence. This is represented by a pair of tokens representing the length of the sequence and the location of the previous occurrence as an offset from the present location. It is worth noting that run-length encoding, where consecutive repetitions of identical sequences of bytes are eliminated, is a special case

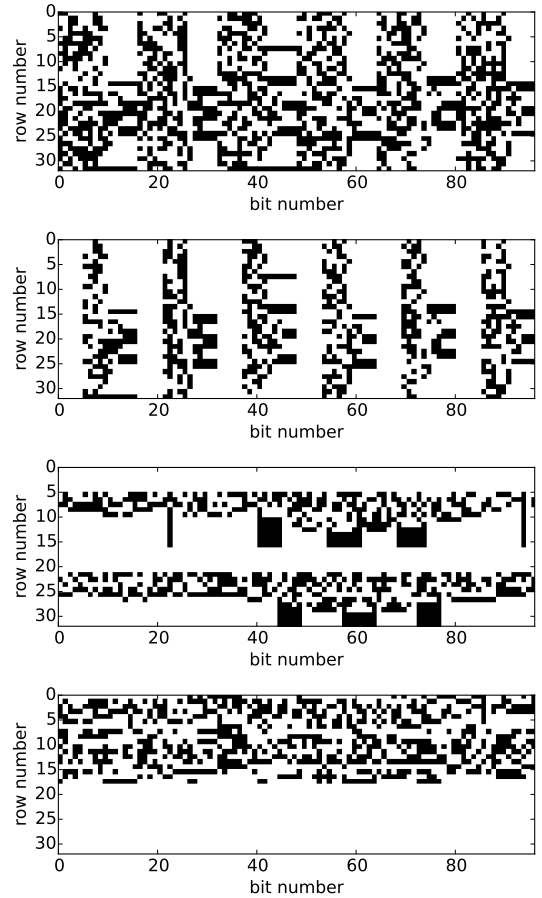


Figure 2: Bit representation of the data in Figure 1 at various stages of compression. The data are stored as an array of two element structs, where each the real and imaginary parts are represented by little-endian signed integers. The data are natively represented by 32-bit integers, but for the compactness of this figure, we divide the data by 2^8 and use 16-bit integers. In all panels, the memory is laid out from left to right (in rows of 96 bits) then top to bottom, with black representing a set bit and white representing an unset bit. Within an 8-bit byte the bits are unpacked from the least significant bit to the most significant bit, which is convenient for visualizing little-endian data types. The panels represent, from top to bottom:

1. The original data with each row containing 3 integrations.
2. Data after reducing precision with $f = 0.01$.
3. Data after the bit-transpose step of **Bitshuffle**. Each column contains a single integration.
4. Data after the LZ4 compression step of **Bitshuffle**.

⁵<http://oldhome.schmorp.de/marc/liblzf.html>

⁶<http://www.oberhumer.com/opensource/lzo/>

⁷<https://code.google.com/p/snappy/>

⁸<https://code.google.com/p/lz4/>

and can be represented by setting the length to be greater than the offset. This class of encoders has the advantage that it can be made very fast, with some implementations (*e.g.* LZ4) achieving greater than 2 GB/s decompression speed on a single core of a modern processor.

The DEFLATE algorithm [23]—best known for its use in both the `gzip` and `zip` programs and file formats—includes LZ77 encoding as a first step, followed by Huffman coding [24]. Huffman coding entails replacing the most commonly occurring byte-values in the uncompressed stream with shorter representations (less than one byte). Less commonly occurring values must be represented using a symbol that is larger than a byte. The LZ77 encoding and Huffman coding are synergetic as they exploit different types of redundancy. Spatial redundancy plays a greater role in LZ77 as the sequence must be an exact match to a previous occurrence, but can be compressed even if the bytes-value within the sequence are rare. The Huffman coding step exploits only the fact that some bytes may be more common than others and compresses data even if these bytes are randomly ordered. Due to the additional Huffman coding step, DEFLATE generally achieves higher compression ratios than the pure LZ77 class encoders. However the computational cost is high and, as we will show, DEFLATE implementations are generally roughly a factor of ten slower than the fastest LZ77 encoders for both compression and decompression.

The above algorithms are representative of those most commonly used for scientific data. Notable omissions are `bzip2`⁹ and LZMA¹⁰, both of which generally achieve higher compression ratios than DEFLATE but were deemed too computationally expensive for high-performance applications.

For *typed* binary data, where the data consist of arrays of elements of a fixed number of bytes, it has been recognized that compression is generally improved by applying the byte reordering `shuffle` pre-filter [25]. `shuffle` breaks apart the bytes of each data element, grouping together all the first (second, etc.) bytes. To put this in other terms, if you arrange all the bytes in the array into a matrix with dimensions of the number of elements by the size of each element, `shuffle` performs a transpose on this matrix. This improves compression ratios, primarily in the LZ77 step, by creating long runs of highly correlated bytes. This relies on consecutive values of the data themselves being highly correlated, but this is broadly the case in scientific data. An illustrative special case is in unsigned integer data that only spans a subset of the representable values. Any unexercised most-significant-bytes are grouped together into a long run of zeros and are trivially compressed.

When paired with the precision reduction described in Section 3, it is expected that it is the Huffman coding that will best exploit the associated reduction of entropy

to achieve a better compression ratio. Even when paired with `shuffle`, the precision reduction does not generically produce long runs of repeated bytes unless eight or more bits are discarded. However, the frequency of certain byte values (multiples of $2^{n_{BT}}$ where n_{BT} is the number of bits discarded) is greatly increased; this is a prime target for Huffman coding.

4.2. Bitshuffle pre-filter and compressor

`Bitshuffle` extends the concept of `shuffle` to the bit level: it arranges the *bits* of a typed data array into a matrix with dimensions of the number of elements by the size of each element (in bits), then performs a transpose. This is illustrated in Panel 3 of Figure 2.

`Bitshuffle` is better able to convert spatial correlations into run-lengths than `shuffle` because it is able to treat correlations within a subset of the bits in a byte instead of only those which apply to the whole byte. It thus allows for the elimination of the computationally expensive Huffman coding step of DEFLATE in favour of the fastest LZ77-class compressor available (we use LZ4). The trade-off is that, because each byte now contains bits from eight neighbouring data elements, spatial correlations must be eight times longer to produce run-lengths of useful length. An illustration of bit-transposed data after compression is shown in Panel 4 of Figure 2.

While the practice is not widely used, we do not claim to be the first to implement bit-transposition of data arrays for the purposes of data compression. In addition to several references to this idea scattered around the World Wide Web, the MAFISC compressor [26] implements bit-transposition as one of its pre-filters.

It is worthwhile to briefly discuss how two’s-complement signed integers are compressed with `Bitshuffle`. In two’s complement, zero is represented by having none of the bits in the element set and -1 is represented by having all of them set. As such, while the values of data having zero crossings may be highly correlated, the bit representations are not. Bit-transposing such datasets does not produce the long runs of zeros or ones in the most significant bits. This can be clearly seen in Panel 3 of Figure 2. As such, it might be expected that such data would not compress well. However, while the sequence of bytes representing the data’s most significant bit (bottom row of Panel 3 of Figure 2) may be incompressible, it is identical to the sequence of bytes representing the second most significant bit (next to bottom row) and so on. As such, the block as a whole turns out to be highly compressible.

4.2.1. Implementation

The bit-transpose operation presented here is computationally more expensive than the byte-transpose in `shuffle` by roughly a factor of four depending on implementation. However, both costs are negligible relative to DEFLATE. `Bitshuffle` implements the bit-transpose using the vectorized SSE2 (present on x86 processors since 2001) and

⁹<http://www.bzip.org/>

¹⁰<http://www.7-zip.org/sdk.html>

AVX2 (present on x86 processors since 2013) instruction sets when available. Using SSE2 instructions, the most computationally expensive part of the bit-transpose can process 16 bytes of data in 24 instructions [27]. Using AVX2 this improves to 32 bytes of data in 24 instructions. In the absence of these instruction sets, the bit-transpose is performed using an algorithm that processes 8 bytes in 18 instructions [28].

For performance reasons, it is beneficial to integrate the lossless compressor, LZ4, directly into `Bitshuffle` rather than applying it as a sequential HDF5 filter. The idea is to bit-transpose a small block of data that fits comfortably into the L1d memory cache and then apply the compressor while it is still in cache. Since getting the memory contents in and out of the cache can be the bottleneck, especially when using multiple threads, this can greatly improve performance. Usually, compressing data in small blocks is detrimental to compression ratios, since the maximum look-back distance for repeated sequences is limited. However, because compression after the bit transpose is trivial, this was found not to be the case for `Bitshuffle`. The default block-size in `Bitshuffle` is 4096 bytes.

`Bitshuffle` is both internally threaded using `OpenMP` and thread safe, making no use of global or static variables. Threading is implemented by distributing blocks among threads.

`Bitshuffle` is written in the C programming language, although it has bindings in Python and is distributed as a Python package. In addition to routines for processing raw buffers, it includes an HDF5 filter which is accessible in Python, can be compiled into a C program, or loaded dynamically using HDF5’s dynamically loaded filters (available in HDF5 version 1.8.11 and later).

5. Evaluation of method

In this section we apply the compression algorithm described above to data from the CHIME Pathfinder to assess the algorithm’s performance and to compare it with other compression schemes. The Pathfinder comprises two parabolic cylinders, each 20m wide by 35m long, with their axes running in a north-south direction. 64 identical dual-polarization feeds are located at 0.3m intervals along the central portion of each focal line.

The data used for the following comparisons was collected on January 25, 2015, starting at roughly 2:10AM PDT. Analogue signals from the CHIME antenna are digitized at 8 bits before being Fourier transformed into spectral channels [14, Section 5] and correlated [29–31]. We include data from 16 correlator inputs connected to four dual-polarization antennas on each of the two cylinders. The dataset includes 1024 time integrations of 21.45s length, 136 correlation products, and a subsample of 64 of the 1024 spectral frequencies uniformly spanning the 400–800 MHz band. The data is arranged such that time is the fastest varying index and frequency the slowest and, as such, the C shape of the array is (64, 136, 1024). Each element is

a struct of two 32-bit, signed, little-endian integers representing the real and imaginary parts of the visibility. The total size of the dataset is $64 \times 136 \times 1024 \times 8$ bytes = 68 MiB.

The data themselves have a rich set of structure, including spectral channels with either persistent or intermittent RFI, a malfunctioning amplifier in one of the 16 signal chains (causing high power and noise in that channel), and the transit of a bright source (the Crab Nebula) as well as part of the Galactic plane. Figure 1 shows a small subset of the dataset including the transit of the Crab Nebula in an inter-cylinder baseline. These data broadly represent the phenomena expected to occur in CHIME data, but statistically will differ significantly from the data produced by the full Pathfinder. With 256 correlator inputs, the data produced by the full Pathfinder will be much more heavily dominated by cross-correlations of long baselines which may have a significant impact on compression.

For all the tests presented below, we use the HDF5 data format and library to perform the compression and store the data. The chunk shape is chosen to be (8, 8, 1024) which gives a total size of 512 KiB.

5.1. Distribution of rounding errors

First we verify that our implementation of the precision reduction behaves as expected when applied to real data. We require that the rounding errors be unbiased, and that the probability distribution of errors be more concentrated than a top-hat function with width of the maximum granularity, given in Equation 16. Rounding errors are calculated by directly subtracting the original dataset from the precision reduced dataset then comparing with the maximum granularity. The distribution of these errors is shown in Figure 3 for various values of f .

The expected probability density is a superposition of top hat functions with widths depending on where the maximum granularity falls relative to a power of two. The function is flat between $\pm 1/4$ since the final power-of-two granularity is always at least half the maximum granularity. As expected, we see that no rounding error exceeds half the maximum granularity in absolute value. For $f = 10^{-5}$ there is an excess of errors at zero as well as a noted jaggedness along the central plateau. This is because, for a significant portion of the data, the granularity is unity, implying no rounding for integers. One might notice that the probability densities for $f = 10^{-5}$ and $f = 10^{-3}$ are nearly identical. This is because these values of f differ by a factor very close to a power of four (4^5) and a scaling relation guarantees identical probability distributions for this case.

The requirement that the rounding be unbiased is satisfied if the probability densities are symmetric about zero, which we have verified is true to within statistical uncertainty from the finite sample. We have also checked for bias in the mean of the errors over time in each frequency

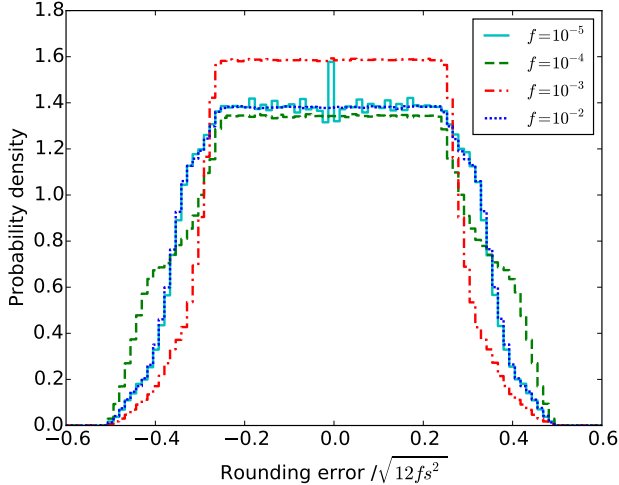


Figure 3: Distribution of rounding errors for different levels of precision reduction. Rounding errors are scaled to the maximum granularity, $\sqrt{12fs^2}$, and the histogram is normalized to integrate to unity and thus approximates the probability density function.

and correlation product, as well as searched for correlations in the errors along the time axis, finding no evidence for either.

We conclude that there is no evidence that the precision reduction is behaving other than expected. Our tests are consistent with it increasing the noise by a fraction of at most f , equivalent to a fractional loss of integration time of f .

5.2. Effectively compressing precision-reduced data

Here, we assess the effectiveness of the precision reduction step and evaluate which subsequent lossless compression algorithms are able to exploit the associated reduction in entropy. In this section, we consider three classes of lossless compression algorithm: the LZ77 class of encoders represented by LZF (chosen due to the availability of an HDF5 filter), the DEFLATE algorithm (implemented in `zlib`¹¹ with compression level 4), and `Bitshuffle`. For the LZF and DEFLATE cases, the `shuffle` pre-filter was applied to the data which was found to improve compression ratios in all cases. We quote compression ratios as the ratio of compressed data size to original data size, expressed as a percentage. Results are shown in Table 1.

It is seen that reducing the precision of the data does in fact improve compression in all cases. Between $f = 10^{-5}$ and $f = 10^{-2}$, the precision of the data is decreased by a factor of $\sqrt{1000}$, or 5.0 bits. Since the data are stored as 32-bit integers, one would optimistically hope for a 15.5% improvement in compression ratio between these cases. All three compressors do a reasonable job of exploiting the reduced entropy, with LZF, DEFLATE, and `Bitshuffle`,

Table 1: Compression ratios for various compression algorithms as a function of degree of precision reduction (parameterized by f , defined in Section 3).

f	LZF	DEFLATE	Bitshuffle
0	69.5%	61.2%	59.6%
10^{-5}	46.7%	38.5%	37.1%
10^{-4}	45.6%	34.1%	32.0%
10^{-3}	44.2%	30.6%	27.9%
10^{-2}	37.1%	25.9%	22.2%

achieving a 9.6%, 12.6%, and 14.9% increase in compression respectively. LZF’s marginally poorer ability to exploit the reduced entropy is in line with our expectations from Section 4.1.

It can be seen that the compression ratio improvements are more uniform for `Bitshuffle` and DEFLATE than for LZF. The former compress by an extra $\sim 4.5\%$ at each step, while LZF sees a much better improvement between $f = 10^{-3}$ and $f = 10^{-2}$. We speculate that this is because `Bitshuffle` and DEFLATE effectively compress each bit as it is discarded, while LZF achieves most of its improvement when the rounding passes a byte-boundary for some portion of the data.

The improvements in compression from the native precision case depend on how much precision is kept by the correlator and data collection software. The CHIME correlator truncates to 4 bits of precision after spectral channelization, with the rest of the correlation process being very nearly lossless. We see that this process keeps an excessive amount of precision, since compression ratios improve by more than 22% even when reducing the precision to a conservative $f = 10^{-5}$. While the precision of the data could in principle be reduced explicitly during acquisition by right-bit-shifting the values by several places, this is much less controlled than comparing to the radiometer equation in the way presented here.

It is worthwhile considering what compression ratio would be achieved if we were to simply reduce the precision then use a minimum data element size. Such a scheme could be conveniently implemented using a custom HDF5 data type along with the N-bit filter. The number of required bits per element is given by $-\log(12f/N)/(2\log 2)$ which, for this data and for $f = 10^{-3}$, is roughly 15 bits. One more bit is required for the sign, and at least one more should be allowed for dynamic range (meaning the total power could change by a factor of two without overflowing), and so such a scheme would achieve a compression ratio just worse than 50%. We see that a mild amount of precision reduction coupled with lossless compression beats this and does not have the complications of tuning scaling factors nor worries about overflows during transits of bright sources or bursts of RFI. In such a scheme changing N , which depends on the integration time and spectral channel bandwidth, would require a change in data type which is inconvenient.

¹¹<http://www.zlib.net/>

In Section 2.2 we argued that ordering the data with time as the fastest varying index is beneficial for compression. To verify this, we repeated the tests in this section using a chunk shape of (64, 32, 32). As expected, all compression ratios worsen. **Bitshuffle** is most sensitive to data ordering with compression ratios worsening by 6% (for $f = 10^{-2}$) to 11% (for $f = 0$), compared to 3% to 4% for the other compressors.

The benefits of the precision reduction are substantial. When compressing with **Bitshuffle**, reducing the precision to $f = 10^{-3}$ more than halves the final data volume.

5.3. Throughput and compression ratios

Here we directly compare several lossless compression schemes on the basis of compression ratio and throughput, fixing the lossy compression at $f = 10^{-3}$. In addition to the **DEFLATE+shuffle** and **LZF+shuffle** schemes presented in the previous section, we compare **Bitshuffle** to **Blosc**¹². **Blosc** is actually a ‘meta-compressor’ which combines an optimized version of the **shuffle** pre-filter with a lossless compressor, using a similar blocking scheme as **Bitshuffle** to optimize the use of the L1d cache. **Blosc** supports several back-end lossless compressors. Here we show results for **LZ4** as well as **LZ4_HC**. **LZ4_HC** is an **LZ4** derivative that uses the same compression format and decompressor as **LZ4** but spends much longer on the compression step in attempt to achieve better compression ratios.

Both **DEFLATE** and **Blosc** have a compression level parameter, whose value can be between 1 (fastest) and 9 (best compression) inclusive. For **DEFLATE** we test levels 1 and 7 to bracket the range of throughputs and compression ratios that can be expected. Levels higher than 7 were found to be excessively slow at compression while not significantly improving compression ratios. For the same reasons we test level 1 for **Blosc+LZ4** and level 5 for **Blosc+LZ4_HC**.

To give an idea of the overhead associated with reading and writing to the datasets, we show the throughput when not compressing the data using both chunked and contiguous storage. Finally, to give an idea of the computational cost of the precision reduction, we include throughputs for the example implementation, although we reiterate the little effort has been put into its optimization.

Benchmarks are for a single thread on an Intel Core i7-3770 CPU running at 3.40GHz. Note that this processor includes support for the SSE2 instruction set but not AVX2. We employ the HDF5 ‘core’ file driver, such that the datasets only ever exist in memory and are never written to disk. Thus the file system plays no role. Our timings are reproducible in repeated trials to within a few percent. Results are presented in Table 2.

We see that **Bitshuffle** obtains a better compression ratio than all other algorithms tested and that only **Blosc**

Table 2: Comparison of the of various compression algorithms on the basis of compression ratios and throughput.

Algorithm	Compression ratio	Write (MiB/s)	Read (MiB/s)
Contiguous	100.0%	5065	2576
Chunked	100.0%	3325	2572
Rounding	100.0%	289	2574
DEFLATE -1	32.2%	73	181
DEFLATE -7	30.3%	23	182
LZF	44.2%	181	245
Blosc+LZ4	47.3%	528	1348
Blosc+LZ4_HC	41.0%	30	1417
Bitshuffle	27.9%	749	1181

outperforms **Bitshuffle** on read throughput. The margin by which **Bitshuffle** outperforms the other compressors is considerable, producing compressed data two thirds the size of the next best ‘fast enough’ (by our requirements in Section 2.2) compressor, **Blosc**. In addition, **Bitshuffle** compresses faster than any compressor tested, which, while not being a design consideration, is a nice bonus. It is not clear why **Bitshuffle** compresses faster than **Blosc+LZ4**, since they use the same back end compressor, use similar block sizes and the **shuffle** pre-filter is much less computationally intensive than **Bitshuffle**’s bit transpose.

For reading, the HDF5 overhead is significant. Both **Blosc** and **Bitshuffle** are within a factor of two of achieving the throughput limits from HDF5. Put another way, the HDF5 overhead accounts for more than half the total time required to read data with these compressors. However, these speeds are all fast compared to hard-drive read-throughputs.

6. Summary and conclusions

We have presented a high-throughput data compression scheme for astronomical radio data that obtains a very high compression ratio. Our scheme includes two parts: reducing the precision of the data in a controlled manner to discard noisy bits, hence reducing the entropy of the data; and the lossless compression of the data using the **Bitshuffle** algorithm.

The entire compression algorithm consists of the following steps, starting with the precision reduction:

1. Estimate the thermal noise on a data-element by data-element basis using Equation 14 in conjunction with the noise covariance matrix defined in either Equation 4 or Equations 5–7
2. Choose an acceptable fractional increase in noise variance f ; we recommend $10^{-5} > f > 10^{-2}$.
3. Round all data to a multiple of the largest possible power of two subject to the limit on rounding granularity given in Equation 16.

¹²<http://www.blosc.org/>

Followed by the lossless compression:

4. Rearrange the bits within blocks of data by arranging them in a matrix with dimensions of the number of elements by the size of each element (in bits), then perform a transpose.
5. Compress with a fast lossless LZ77 style compressor.

The lossless compression is implemented and distributed as the **Bitshuffle** software package which includes an HDF5 filter for the algorithm and bindings for the C and Python programming languages.

We reiterate that the precision reduction and **Bitshuffle** lossless compression steps are independent. They work very well together, however, we have shown that several commonly available lossless compression algorithms are able to exploit the reduction of information entropy associated with precision reduction. In addition, we have shown that **Bitshuffle** performs very well compared to other lossless compressors with and without the precision reduction.

The algorithms in this paper use integers, since the CHIME experiment produces and records visibility data in integer representation. However, most of the aforementioned procedures and conclusions apply equally well to floating-point data. Reducing the precision of floating point numbers entails adapting the rounding procedure to act only on the significand, and **Bitshuffle** works for any data type with no modifications. It is not expected that floating point numbers will compress as well as integers under this scheme, especially for data with frequent zero crossings. In such data there can be large fluctuations in the exponent, inhibiting compression. This can especially affect interferometer data where cross correlations over long baselines are often zero within noise.

In addition to our compression scheme we present the following considerations for developing a data storage format for high performance applications:

- Because decompression can be fast compared to reading data from disk, compression can improve IO performance.
- Compression and HDF5 chunking should not reduce the speed of random access data reads for files stored on hard disks since the disk seek time is generally longer than the time required to read and decompress the data.
- Data are generally read more often than they are written, and as such read performance should be prioritized over write performance. For this reason, a post-acquisition data reordering step can be worthwhile.
- Data consumer usage patterns should be the primary consideration when deciding a data layout. For CHIME this means having time as the minor (fastest varying) axis. This is also beneficial for compression

ratios when using **Bitshuffle** since time is the axis over which the data are most highly correlated.

We have shown that when applying our compression scheme to data produced by the CHIME experiment, the data are compressed to 28% of their original size which in many cases will improve read performance by over a factor of three. In addition we have shown that **Bitshuffle**, when applied to CHIME data, outperforms all compression algorithms tested in both throughput and compression ratios.

The benefits of our compression scheme are substantial with essentially no drawbacks. The CHIME experiment is employing the algorithm in a post-acquisition data re-ordering and compression step that creates our final archive files. As radio datasets continue to grow in size, more instruments will need to employ compression to keep these datasets manageable. We expect that our scheme is broadly applicable to most post-correlation radio data, and that aspects of it could benefit many current and future instruments should the change in data format be deemed worthwhile.

Acknowledgments

We are very grateful for the warm reception and skillful help we have received from the staff of the Dominion Radio Astrophysical Observatory, operated by the National Research Council Canada.

CHIME is Leading Edge Fund project 31170 funded by the Canada Foundation for Innovation, the B.C. Knowledge Development Fund, le Cofinancement gouvernement du Québec-FCI, and the Ontario Research Fund. K. Masui is supported by the Canadian Institute for Advanced Research, Global Scholars Program. M. Deng acknowledges a MITACS fellowship. We acknowledge support from the Natural Sciences and Engineering Research Council of Canada, the CfAR Cosmology and Gravity program, the Canada Research Chairs program, and the National Research Council of Canada. We thank Xilinx and the XUP for their generous donations.

References

References

- [1] J. C. Pober, A. R. Parsons, D. R. DeBoer, P. McDonald, M. McQuinn, J. E. Aguirre, Z. Ali, R. F. Bradley, T.-C. Chang, M. F. Morales, The Baryon Acoustic Oscillation Broadband and Broad-beam Array: Design Overview and Sensitivity Forecasts, *AJ*145 (2013) 65.
URL <http://bao.berkeley.edu/>
- [2] R. A. Battye, I. W. A. Browne, C. Dickinson, G. Heron, B. Maffei, A. Pourtsidou, H I intensity mapping: a single dish approach, *MNRAS*434 (2013) 1239–1256.
- [3] The CHIME Collaboration, Canadian Hydrogen Intensity Mapping Experiment (CHIME) (2015).
URL <http://chime.phas.ubc.ca/>

- [4] J. C. Pober, A. Liu, J. S. Dillon, J. E. Aguirre, J. D. Bowman, R. F. Bradley, C. L. Carilli, D. R. DeBoer, J. N. Hewitt, D. C. Jacobs, M. McQuinn, M. F. Morales, A. R. Parsons, M. Tegmark, D. J. Werthimer, What Next-generation 21 cm Power Spectrum Measurements can Teach us About the Epoch of Reionization, *ApJ*782 (2014) 66.
- [5] L. J. Greenhili, D. Werthimer, G. B. Taylor, S. W. Ellingson, A broadband 512-element full correlation imaging array at VHF (LEDA), in: 2012 International Conference on Electromagnetics in Advanced Applications, Institute of Electrical & Electronics Engineers (IEEE), 2012, pp. 1117–1120.
URL <http://dx.doi.org/10.1109/ICEAA.2012.6328797>
- [6] M. P. van Haarlem, M. W. Wise, A. W. Gunst, G. Heald, J. P. McKean, J. W. T. Hessels, A. G. de Bruyn, R. Nijboer, J. Swinbank, R. Fallows, et al., LOFAR: The LOW-Frequency ARray, *A&A*556 (2013) A2.
URL <http://www.lofar.org/>
- [7] H. Zheng, M. Tegmark, V. Buza, J. S. Dillon, H. Gharibyan, J. Hickish, E. Kunz, A. Liu, J. Losh, A. Lutomirski, S. Morrison, S. Narayanan, A. Perko, D. Rosner, N. Sanchez, K. Schutz, S. M. Tribiano, M. Zaldarriaga, K. Zarb Adami, I. Zelko, K. Zheng, R. Armstrong, R. F. Bradley, M. R. Dexter, A. Ewall-Wice, A. Magro, M. Matejek, E. Morgan, A. R. Neben, Q. Pan, C. M. Peterson, M. Su, J. Villasenor, C. L. Williams, H.-I. Yang, Y. Zhu, Mapping our universe in 3D with MITEoR, in: 2013 IEEE International Symposium on Phased Array Systems & Technology, IEEE, 2013, pp. 784 – 791.
- [8] A. R. Parsons, D. C. Backer, G. S. Foster, M. C. H. Wright, R. F. Bradley, N. E. Gugliucci, C. R. Parashare, E. E. Benoit, J. E. Aguirre, D. C. Jacobs, C. L. Carilli, D. Herne, M. J. Lynch, J. R. Manley, D. J. Werthimer, The Precision Array for Probing the Epoch of Re-ionization: Eight Station Results, *AJ*139 (2010) 1468–1480.
URL <http://eor.berkeley.edu/>
- [9] X. Chen, The Tianlai Project: a 21CM Cosmology Experiment, *International Journal of Modern Physics Conference Series* 12 (2012) 256–263.
URL <http://tianlai.bao.ac.cn/>
- [10] S. Johnston, R. Taylor, et al., Science with ASKAP. The Australian square-kilometre-array pathfinder, *Experimental Astronomy* 22 (2008) 151–273.
- [11] C. J. Lonsdale, R. J. Cappallo, M. F. Morales, F. H. Briggs, L. Benkevitch, J. D. Bowman, J. D. Bunton, S. Burns, B. E. Corey, L. Desouza, S. S. Doeleman, M. Derome, A. Deshpande, M. R. Gopala, L. J. Greenhill, D. E. Herne, J. N. Hewitt, P. A. Kamini, J. C. Kasper, B. B. Kincaid, J. Kocz, E. Kowald, E. Kratzenberg, D. Kumar, M. J. Lynch, S. Madhavi, M. Matejek, D. A. Mitchell, E. Morgan, D. Oberoi, S. Ord, J. Pathikulangara, T. Prabu, A. Rogers, A. Rosh, J. E. Salah, R. J. Sault, N. U. Shankar, K. S. Srivani, J. Stevens, S. Tingay, A. Vaccarella, M. Waterson, R. B. Wayth, R. L. Webster, A. R. Whitney, A. Williams, C. Williams, The Murchison Widefield Array: Design Overview, *IEEE Proceedings* 97 (2009) 1497–1506.
URL <http://www.mwatelescope.org/>
- [12] R. S. Booth, W. J. G. de Blok, J. L. Jonas, B. Fanaroff, MeerKAT Key Project Science, Specifications, and Proposals, *ArXiv e-prints*.
- [13] The SKA Organization, The Square Kilometer Array (2015).
URL <http://www.skatelescope.org>
- [14] K. Bandura, G. E. Addison, M. Amiri, J. R. Bond, D. Campbell-Wilson, L. Connor, J.-F. Cliche, G. Davis, M. Deng, N. Denman, M. Dobbs, M. Fandino, K. Gibbs, A. Gilbert, M. Halpern, D. Hanna, A. D. Hincks, G. Hinshaw, C. Höfer, P. Klages, T. L. Landecker, K. Masui, J. Mena Parra, L. B. Newburgh, U.-L. Pen, J. B. Peterson, A. Recnik, J. R. Shaw, K. Sigurdson, M. Sitwell, G. Smecher, R. Smegal, K. Vanderlinde, D. Wiebe, Canadian Hydrogen Intensity Mapping Experiment (CHIME) pathfinder, in: *Society of Photo-Optical Instrumentation Engineers (SPIE) Conference Series*, Vol. 9145 of *Society of Photo-Optical Instrumentation Engineers (SPIE) Conference Series*, 2014, p. 22.
- [15] L. B. Newburgh, G. E. Addison, M. Amiri, K. Bandura, J. R. Bond, L. Connor, J.-F. Cliche, G. Davis, M. Deng, N. Denman, M. Dobbs, M. Fandino, H. Fong, K. Gibbs, A. Gilbert, E. Griffin, M. Halpern, D. Hanna, A. D. Hincks, G. Hinshaw, C. Höfer, P. Klages, T. Landecker, K. Masui, J. M. Parra, U.-L. Pen, J. Peterson, A. Recnik, J. R. Shaw, K. Sigurdson, M. Sitwell, G. Smecher, R. Smegal, K. Vanderlinde, D. Wiebe, Calibrating CHIME: a new radio interferometer to probe dark energy, in: *Society of Photo-Optical Instrumentation Engineers (SPIE) Conference Series*, Vol. 9145 of *Society of Photo-Optical Instrumentation Engineers (SPIE) Conference Series*, 2014, p. 4.
- [16] The HDF Group, Hierarchical Data Format, version 5 (1997–2015).
URL <http://www.hdfgroup.org/HDF5/>
- [17] A. R. Thompson, J. M. Moran, G. W. Swenson, Jr., *Interferometry and Synthesis in Radio Astronomy*, 2nd Edition, Wiley, 2001.
- [18] S. R. Kulkarni, Self-noise in interferometers - Radio and infrared, *AJ*98 (1989) 1112–1130.
- [19] The IEEE, Standard for floating-point arithmetic, *IEEE Std.* 754-2008.
- [20] B. Lathi, *Modern Digital and Analog Communication Systems*, The Oxford series in electrical and computer engineering, Oxford University Press, 1998.
- [21] J. Ziv, A. Lempel, A universal algorithm for sequential data compression, *IEEE Transactions on Information Theory* 23 (3) (1977) 337–343.
URL <http://dx.doi.org/10.1109/TIT.1977.1055714>
- [22] J. Ziv, A. Lempel, Compression of individual sequences via variable-rate coding, *IEEE Transactions on Information Theory* 24 (5) (1978) 530–536.
URL <http://dx.doi.org/10.1109/TIT.1978.1055934>
- [23] L. P. Deutsch, DEFLATE Compressed Data Format Specification version 1.3, RFC 1951, RFC Editor (May 1996).
URL <http://www.rfc-editor.org/rfc/rfc1951.txt>
- [24] D. Huffman, A method for the construction of minimum-redundancy codes, *Proceedings of the IRE* 40 (9) (1952) 1098–1101.
URL <http://dx.doi.org/10.1109/JRPROC.1952.273898>
- [25] The HDF Group, Shuffle Performance, accessed: Jan 2015 (1997–2015).
URL http://www.hdfgroup.org/HDF5/doc_resource/H5Shuffle_Perf.pdf
- [26] N. Hübbe, J. Kunkel, Reducing the HPC-datastorage footprint with MAFISC—multidimensional adaptive filtering improved scientific data compression, *Computer Science - Research and Development* 28 (2-3) (2012) 231–239.
URL <http://dx.doi.org/10.1007/s00450-012-0222-4>
- [27] M. Sandberg, What is SSE !@# good for? Transposing a bit matrix, accessed: Jan 2015 (July 2011).
URL <https://mischasan.wordpress.com/2011/07/24/what-is-sse-good-for-transposing-a-bit-matrix/>
- [28] H. S. J. Warren, *Hacker’s Delight*, Addison-Wesley, 2002.
- [29] N. Denman, M. Amiri, K. Bandura, J.-F. Cliche, L. Connor, M. Dobbs, M. Fandino, M. Halpern, A. Hincks, G. Hinshaw, C. Höfer, P. Klages, K. Masui, J. Mena Parra, L. Newburgh, A. Recnik, J. R. Shaw, K. Sigurdson, K. Smith, K. Vanderlinde, A GPU-based Correlator X-engine Implemented on the CHIME Pathfinder, *ArXiv e-prints*.
- [30] P. Klages, K. Bandura, N. Denman, A. Recnik, J. Sievers, K. Vanderlinde, GPU Kernels for High-Speed 4-Bit Astrophysical Data Processing, *ArXiv e-prints*.
- [31] A. Recnik, K. Bandura, N. Denman, A. D. Hincks, G. Hinshaw, P. Klages, U.-L. Pen, K. Vanderlinde, An Efficient Real-time Data Pipeline for the CHIME Pathfinder Radio Telescope X-Engine, *ArXiv e-prints*.